chemistry

MDPI

Article

Experimental and Computational Studies on *N*-alkylation Reaction of *N*-Benzoyl 5-(Aminomethyl)Tetrazole

Younas Aouine [1,2,*], Aaziz Jmiai [3,*], Anouar Alami [2], Abdallah El Asri [3], Souad El Issami [3] and Idriss Bakas [4]

[1] Team of Organic Chemistry and Valorization of Natural Substances (COVSN), Faculty of Sciences, Ibn Zohr University, P.O. Box 8106 Cité Dakhla, Agadir 80000, Morocco
[2] Laboratory Engineering Laboratory of Organometallic, Molecular Materials and Environment (LIMOME), Faculty of Sciences, Sidi Mohammed Ben Abdellah University, Fez 30000, Morocco; alamianouar@yahoo.fr
[3] Applied Physical Chemistry and Environment Team, Faculty of Sciences, Ibn Zohr University, P.O. Box 8106 Cité Dakhla, Agadir 80000, Morocco; elasriabdallah4@gmail.com (A.E.A.); s.elissami19@gmail.com (S.E.I.)
[4] Team Catalysis and Environment, Faculty of Sciences, Ibn Zohr University, P.O. Box 8106 Cité Dakhla, Agadir 80000, Morocco; idrissbakas@gmail.com
* Correspondence: aouineyounas@yahoo.fr (Y.A.); jmiai.aziz@gmail.com (A.J.); Tel.: +212-637374200 (Y.A.); +212-665150480 (A.J.)

Abstract: The *N*-alkylation reaction of *N*-benzoyl 5-(aminomethyl)tetrazole (5-AMT) with benzyl bromide was carried out in the presence of K_2CO_3 as a base. Two separable regioisomers were obtained, thus their purification led to determine the proportion of each of them, and their structures were attributed essentially based on ^{1}H and ^{13}C NMR spectroscopy in addition to the elemental analysis and MS data. In order to confirm the results obtained at the synthesis level, a computational study was carried out by application of density functional theory (DFT) using the Becke three-parameter hybrid exchange functional and the Lee-Yang-Parr correlation functional (B3LYP).

Keywords: tetrazole; tautomerism; *N*-alkylation; NMR; DFT

Citation: Aouine, Y.; Jmiai, A.; Alami, A.; El Asri, A.; El Issami, S.; Bakas, I. Experimental and Computational Studies on *N*-alkylation Reaction of *N*-Benzoyl 5-(Aminomethyl)Tetrazole. *Chemistry* **2021**, *3*, 704–713. https://doi.org/10.3390/chemistry3030049

Academic Editor: Luis R. Domingo

Received: 10 May 2021
Accepted: 28 June 2021
Published: 5 July 2021

1. Introduction

Tetrazole and its derivatives have attracted much attention because of their unique structure and applications in numerous fields. Tetrazole is associated with different biological activities, such as antibacterial [1], anticancer [2], antifungal [3,4], anti-inflammatory [5], antimalarial [6], antitubercular [7] and antiviral [8]. Indicatively, tetrazole derivatives are investigated both as potential explosives and as rocket propellant components based on their high energy properties [9,10]; Moreover, tetrazoles, due to their high number of nitrogen atoms, could serve as an environmentally benign component of gas generators with a high burn rate and relative stability [11].

The isosteric similarities of tetrazole and carboxylate anions have been provided by computational evidence [12] but over the past decades, it has as well been established that 5-substituted 1*H*-tetrazoles are effective (bio)isosteres of the carboxylic acid functionality [13,14]. The acidity of N-H is similar to that of O-H at physiological *p*H, both exhibits planar structures, tetrazoles being more lipophilic; key factor when crossing cell membranes; than the corresponding carboxylic analogs [15,16].

It exists in two tautomeric forms, 1*H*- and 2*H*-form (Scheme 1), in which the 1*H*-form is more stable and predominant in solution, while the 2*H*-form is more stable in the gas phase [17,18]. Tetrazole has the highest ionization potential (11.3 eV) and the dipole moment in dioxane is 5.15 D. Tetrazole is acidic in nature and its pKa of 4.89 is comparable to acetic acid (pKa 4.76).

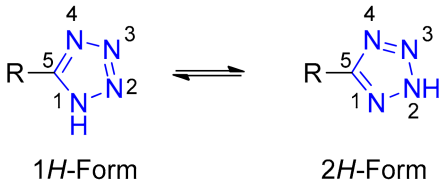

Scheme 1. Tautomerism of Tetrazole Derivatives.

Understanding the changes and mechanisms of reactions during a chemical reaction is not easy. For this reason, quantum and theoretical chemistry is important to examine the molecular reactivity of organic compounds whether "products or reactants". The synthesis of natural chemical compounds increasingly uses theoretical and computational chemistry approaches to understand structural and energetic molecular phenomena [19]. Density Functional Theory (DFT) provides a fruitful framework for exploring a conceptual theory of chemical reactivity [20–22].

The objective of this work is to study the N-alkylation reaction of *N*-benzoyl 5-(aminomethyl)-tetrazole (5-AMT) with benzyl bromide in an alkaline medium. The structures of the regioisomers obtained were assigned essentially on basis of (^{1}H and ^{13}C) NMR spectroscopy in addition to the elemental analysis and MS data. We have also presented theoretical justifications for the *N*-alkylation of (5-AMT) with benzyl bromide observed experimentally. In this sense, we have examined the nucleophility, electrophility and electrostatic potential (ESP) of the reagents used. As well as the stability and reactivity of the products found.

2. Materials and Methods

Melting points were determined with an Electrothermal melting point apparatus and are uncorrected. NMR spectra (^{1}H, ^{13}C) were recorded on a Bruker AM 300 (operating at 300.13 MHz for ^{1}H, and at 75.47 MHz for ^{13}C) spectrometer (Cité d'Innovation, Fez, Morocco). NMR data are listed in ppm and are reported relative to tetramethylsilane; residual solvent peaks being used as internal standard and coupling constants (*J*) are given in hertz. TLC analyses were carried out on 0.25 mm thick precoated silica gel plates (Merck Fertigplatten Kieselgel 60F_{254}) and spots were visualized under UV light or by exposure to vaporized iodine. Mass spectra were recorded on a PolarisQ Ion Trap GC/MS Mass Spectrometer (Cité d'Innovation, Fez, Morocco). Elemental analyses were done in Central Service of Analysis at Rabat.

To a solution of 10 mmol of *N*-((tetrazol-5-yl)methyl)benzamide (5-AMT) and 25 mL of anhydrous acetone, 11 mmol of K_2CO_3 were added under stirring for 15 min, then 10 mmol of benzyl bromide were added. The reaction mixture was stirred at room temperature for 2 h. After the reaction, the solvent was evaporated and the obtained residue was taken up in ethyl acetate, washed into the water three times. Organic layers were combined, dried with Na_2SO_4, evaporated and purified by column chromatography on silica gel (eluent: ether/hexane: 3/2). Yield = 74%.

N-((1-benzyl-1*H*-tetrazol-5-yl)methyl)benzamide (1,5-AMT): white solid; m.p. = 104–106 °C; Ratio of 1*H*-regioisomer = 45%; R_f = 0.48 (ether). δ_H(ppm, DMSO, 300.13 MHz): 4.81 (2H, -CH_2-Tet, d, *J* = 5.70); 5.75 (2H, -CH_2-Ph, s); 7.26–7.82 (10H_{arom}, m); 9.28 (1H, -NH-CO, t, *J* = 5.70). δ_C(ppm, DMSO, 75.47 MHz): 33.02 (-CH_2-Tet); 50.41 (-CH_2-Ph); 127.77–135.02 (12C_{arom}); 153.87 (-C_q(Tet)); 167.12(CO_{amide}). MS-EI: $[M + 1]^+$ = 294. Elemental analysis: Calcd.: C 65.52, H 5.12, N 23.89; Found: C 65.08, H 5.31, N 23.45.

N-((2-benzyl-2*H*-tetrazol-5-yl)methyl)benzamide (2,5-AMT): white solid; m.p. = 88–90 °C; Ratio of 2*H*-regioisomer = 55%; R_f = 0.58 (ether). δ_H(ppm, DMSO, 300.13 MHz): 4.71 (2H, -CH_2-Tet, d, *J* = 5.70); 5.90 (2H, -CH_2-Ph, s); 7.33–7.88 (10H_{arom}, m); 9.19 (1H, -NH-CO, t, *J* = 5.70). δ_C(ppm, DMSO, 75.47 MHz): 34.96 (-CH_2-Tet); 56.29 (-CH_2-Ph); 127.76–134.60 (12C_{arom}); 164.94 (-C_q(Tet)); 166.69 (CO_{amide}). MS-EI: $[M + 1]^+$ = 294. Elemental analysis: Calcd.: C 65.52, H 5.12, N 23.89; Found: C 65.87, H 5.29, N 23.29.

3. Results

Generally, organic reactions are classified as nonpolar or polar; this depends on the overall electronic nature of the bond break and/or the bond formed during the reaction. The nucleophilic or electrophilic power of a molecule is obviously linked to its capacity to exchange electron density with a reaction. So the protocol for understanding this chemical mechanism requires taking into consideration the electronic structure of the system, which could only be possible with quantum description. With the application of theoretical chemistry based on quantum mechanics, it is possible to obtain several theoretical parameters such as electronic parameters (Electrostatic potential, orbital energies (Lowest unoccupied molecular orbital (LUMO) and highest occupied molecular orbital (HOMO)), Energy gap (energy difference between E_{LUMO} and E_{HOMO}), electrophilicity, nucleophilicity . . .), energy parameters (enthalpy of formation).

The HOMO and LUMO energies found can be used for the calculation of other parameters related to the stability of the molecule such as the electronic chemical potential (μ), the chemical softness (S), the chemical hardness (η), the electrophilicity index (ω) and nucleophilicity index (N). These can be calculated as follows:

-Electronic Chemical Potential [23]:

$$(\mu) = -(\chi) = (E_{HOMO} + E_{LUMO})/2 \quad (1)$$

-Chemical Hardness:

$$(\eta) = (E_{LUMO} - E_{HOMO}) \quad (2)$$

-Electrophilicity Index:

$$(\omega) = \mu^2/2\eta \quad (3)$$

And molecular softness [24]:

$$(S) = 1/2\eta \quad (4)$$

-The nucleophilicity index N is referenced to the HOMO energy of tetracyanoethylene (TCE) [25]:

$$N = E_{HOMO}\,(Nu) - E_{HOMO}\,(TCE) \quad (5)$$

The molecules studied were created using Gaussian View software version 5.0.8. The optimization of the geometry and the quantum parameters found were carried out in the aqueous phase using Gaussian 09 software [26]. The solvent effect is treated based on the IEFPCM model (Integral Equation Formalism Polarizable Continuum Model) using water as solvent [27].

DFT calculations were carried out using the Becke three-parameter hybrid exchange functional and the Lee-Yang-Parr correlation functional (B3LYP) together with 6-31G (d) basis [28,29]. All calculations are done in the aqueous phase.

4. Discussion

4.1. Experimental

The compound 5-AMT was obtained in high yield [30]. However, the control of its purity by the Thin-Layer Chromatography (TLC) showed that there was only a very thin trail, which proved that the 5-AMT in the form of an inseparable mixture of two tautomeric forms 1*H* and 2*H*. In order to have an idea on the ratio of each resulting regioisomers from its *N*-alkylation, we performed this reaction with benzyl bromide in the presence of K_2CO_3 as base (Scheme 2).

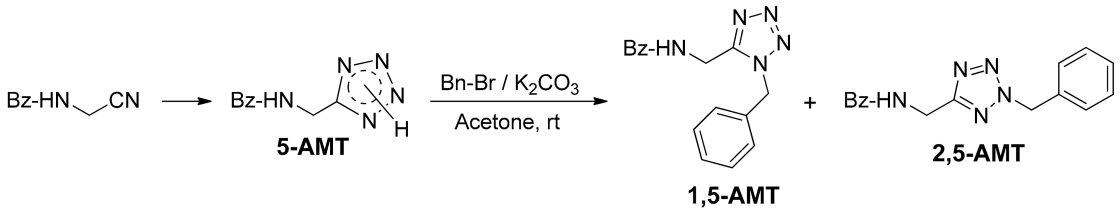

Scheme 2. *N*-alkylation strategy of 5-AMT.

After reaction, the control of the crude product by TLC showed the appearance of two distant spots between them, which easily led to the separation of these two formed regioisomers by column chromatography of silica gel to determine the ratio of each of them.

The structures of the 5-AMT (Figure 1) and two regioisomers 1,5-AMT and 2,5-AMT will be definitively established on the basis of the study of the NMR spectra (^{1}H, ^{13}C) of the two obtained compounds (Figures 2 and 3).

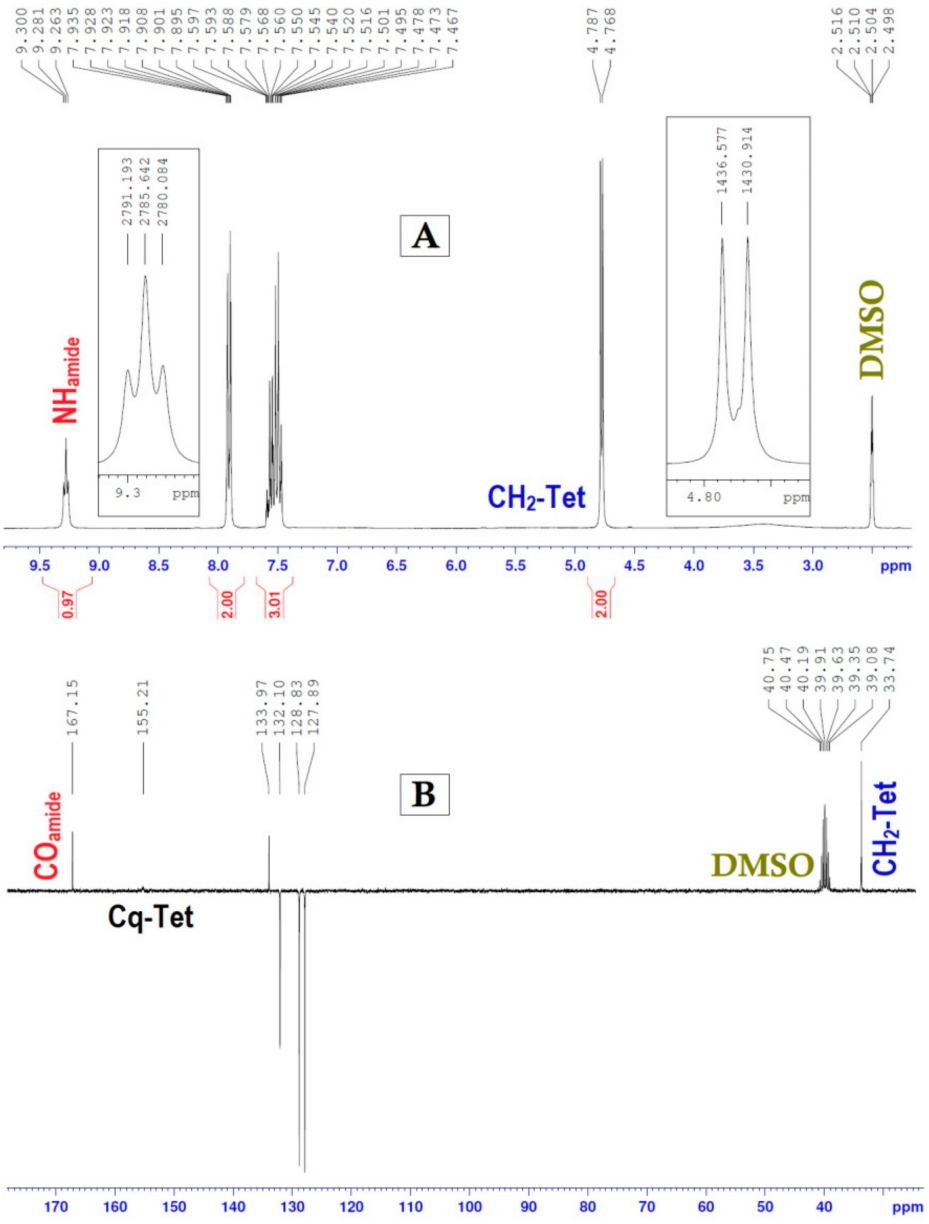

Figure 1. ^{1}H (**A**) and ^{13}C NMR (**B**) spectra of 5-AMT.

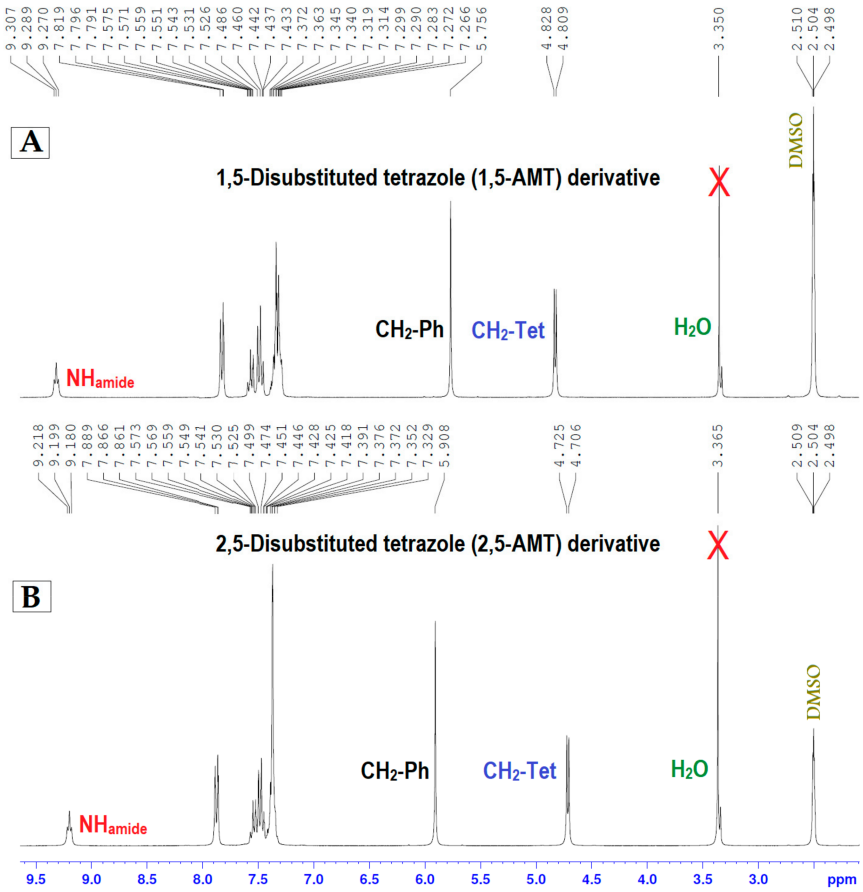

Figure 2. ^{1}H NMR spectra, (**A**) of 1,5-AMT and (**B**) of 2,5-AMT.

In the case of the derivative (1,5-AMT), the benzene ring is located just below the rest of the molecule, which will influence the environment of the methylene protons -CH_2-Tet as well as the amide proton -NH-CO, hence its contribution to modifying their local magnetic fields.

It is, therefore, a weak magnetic anisotropy near the benzene ring, resulting from the electronic current, which associated with the delocalization of the electrons (π), on either side of the plane of the benzene ring. This translates to a light deshielding of these protons -CH_2-Tet and -NH-CO. On the other hand, the two methylene protons -CH_2-Ph are this time deshielding in the case of the derivative (2,5-AMT) thanks to their more electronegative environment.

The ^{1}H NMR spectrum of the derivative (1,5-AMT) shows a doublet at 4.81 ppm attributed to the methylene protons -CH_2-Tet (J = 5.70247 Hz) and a triplet at 9.29 ppm corresponding to the amide proton -NH-CO (J = 5.70247 Hz) (Table 1). Likewise, the ^{1}H NMR spectrum of the derivative (2,5-AMT) also presents a doublet at 4.71 ppm attributed to the methylene protons -CH_2-Tet (J = 5.70247 Hz) and a triplet at 9.19 ppm corresponding to the amide proton -NH-CO (J = 5.70247 Hz).

Table 1. ^{1}H Chemical shift assignments (in ppm) and coupling constants (in Hz) in 1,5- and 2,5-AMTs derivatives (DMSO-d_6).

	1,5-AMT	**2,5-AMT**
−CH_2-Tet	4.81 (J = 5.70247)	4.71 (J = 5.70247)
−CH_2-Ph	5.75	5.90
−NH-CO	9.29 (J = 5.70247)	9.19 (J = 5.70247)

According to the measured values of the coupling constant (*J*) in all cases and to the multiplicity of the signals, the protons −CH_2-Tet and −NH-CO are coupled in the case of the two derivatives.

Since the chemical shifts of these two types of protons are slightly influenced by the phenomenon of anisotropy due to the precession cone of the aromatic cycle in the case of 1,5-AMT, the coupling constant (*J*) remains unchanged, which shows again that the spin-spin coupling is independent of the applied magnetic field.

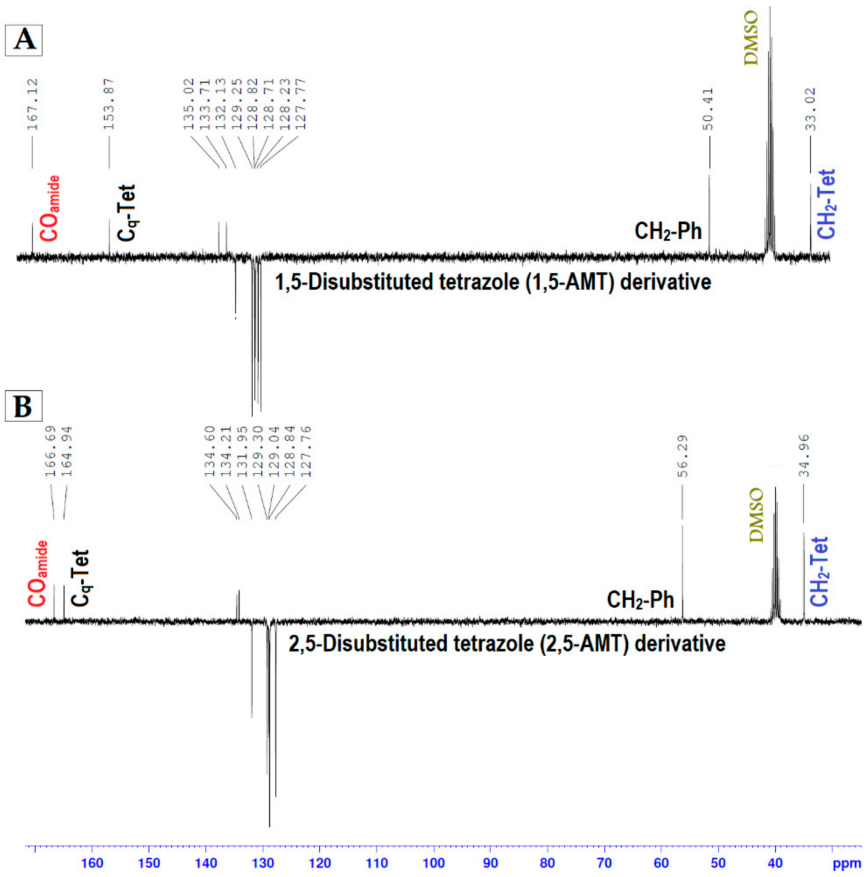

Figure 3. ^{13}C NMR spectra, (**A**) of 1,5-AMT and (**B**) of 2,5-AMT.

The ^{13}C NMR spectra of the two derivatives 1,5-AMT and 2,5-AMT respectively present, inter alia, the signals corresponding to the tetrazole's carbon -C_q(Tet) at 153.87 ppm and 164.94 ppm (Table 2). In general, the C_q signal of tetrazoles is deshielded by about 9.2–12.2 ppm in 2,5-disubstituted derivatives relative to the corresponding 1,5-disubstituted derivatives [31,32]. Hence, regioisomers' structures 1,5-AMT and 2,5-AMT have been well proposed. After purification on a silica gel column, the two regioisomers 1,5-AMT and 2,5-AMT were obtained with slightly different proportions. This suggests that the 5-AMT, which contains a free N-H bond, has existed as a 1:1 ratio of 1*H*- and 2*H*-tautomeric forms, but in reality, with a slight predominance of 2*H*-form [32].

Table 2. ^{13}C Chemical shift assignments (in ppm) in 1,5- and 2,5-AMTs derivatives (DMSO-d_6).

	1,5-AMT	**2,5-AMT**
−CH_2-Tet	33.02	34.96
−CH_2-Ph	50.41	56.29
−C_q(Tet)	153.87	164.94

4.2. Computational Calculation

Figure 4 shows the optimized geometries and representations of the electrostatic potential (Isosurface) of the reagents studied. The examination of Electrostatic potential ESP maps (Isosurface representation). The high electronic density is represented by a red (Isosurface) color, and the low electronic density is represented by a blue (Isosurface) color. It can be clearly seen in this Figure that the regions of negative potential in red colors (Isosurface), are delocalized in the nucleophiles sites of the molecules tested. On the other hand, the zones of positive potential in blue colors (Isosurface) are mainly distributed near the electrophile sites. This really means that its two regions in blue are the two sites responsible for the attack and reactivity of two molecules with the benzyl bromide.

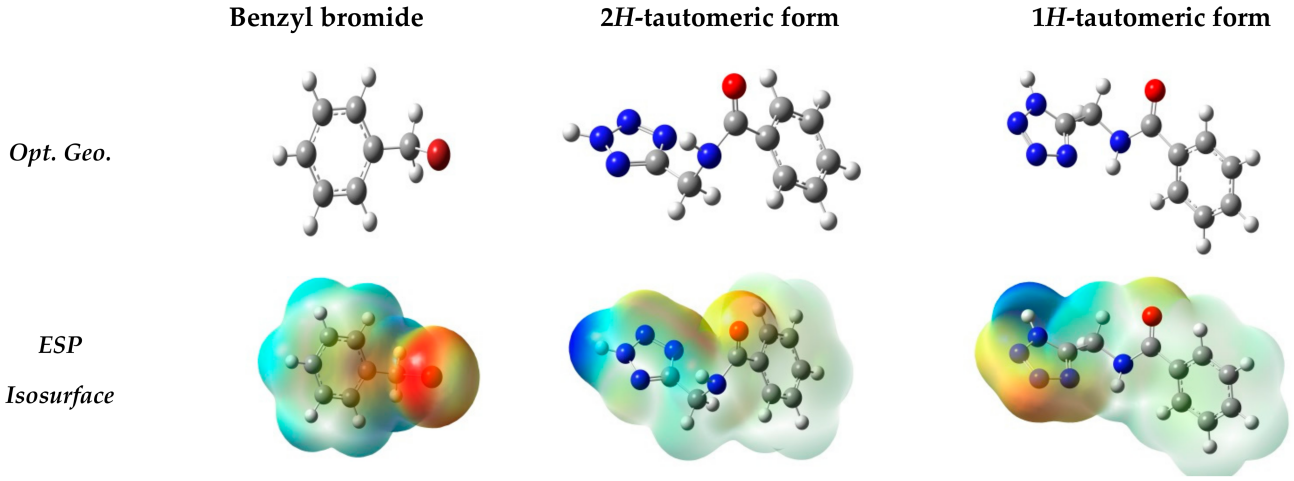

Figure 4. The optimized geometry and representations of electrostatic potential (Isosurface) of the studied compounds.

Many studies of organic reactions have shown that the analysis of reactivity indices to determine from density the conceptual functional theory (CDFT). The global DFT reactivity indices, namely the chemical hardness η, indices of electronic chemical potential μ, softness S, electrophilicity ω and nucleophilicity N of the reagents, are given in Table 3.

Table 3. Electronic chemical potential μ, chemical hardness η, electrophilicity ω, nucleophilicity N and softness S calculated using DFT/B3LYP/6-31G (d) (eV).

	Reaction 1 (1,5-AMT)		**Reaction 2 (2,5-AMT)**	
	1*H*-Form	**Benzyl Bromide**	**2*H*-Form**	**Benzyl Bromide**
μ	−1.56	−1.50	−1.67	−1.50
η	5.30	6.64	4.67	6.64
S	0.09	0.075	0.10	0.07
ω	0.13	0.17	0.12	0.17
N	4.93	4.32	5.13	4.32

This table indicates that the electrophilic and nucleophilic character of 1*H*- and 2*H*-tautomeric forms are different. The electronic chemical potential analysis of two forms; 1*H*-form (μ = −1.56 eV), 2*H*-form (μ = −1.67 eV), and of benzyl bromide (μ = −1.50 eV) indicates that benzyl bromide has greater energy than the two forms. This suggests that reaction 2 between benzyl bromide and the 2*H*-tautomeric form will have a high polar character, compared to reaction 1. To fully explain the reactivity of the two forms with benzyl bromide, we compared the nucleophilicity N and the electrophilicity ω. An N nucleophilicity of 2*H*-form (5.13 eV) is stronger than 1*H*-form (4.93 eV) compared to benzyl bromide (4.32 eV). Regarding the electrophilicity ω, benzyl bromide (0.17 eV) is stronger

than both forms; 1*H*-form (0.13 eV), and 2*H*-form (0.12 eV). From this table, we noticed that the two compounds 1*H*- and 2*H*-tautomeric forms are strong nucleophiles witch react with the electrophile "benzyl bromide" to form the two products (1,5- and 2,5-AMT). We have also found that the compound 2,5-AMT is the slightly majority product and 1,5-AMT is the minority, this is justified by the significant nucleophilicity of 2*H*-form than 1*H*-form. This explains the experimental results obtained i.e., 55% 2,5-AMT and 45% 1,5-AMT.

Theoretical reactivity indices defined within the CDFT [29], we can examine the electrophilic/nucleophilic character. The highest occupied molecular orbital (HOMO) is an electron donor system (nucleophile) to another receptor system, while the lowest unoccupied molecular orbital (LUMO) is an electron acceptor (electrophile). The gap energy ΔE_{gap} or (E_{HOMO}-E_{LUMO}) gives information on the reactivity of the system; if ΔE_{gap} is low, means that the system is reactive and stable, i.e. the electrons transfer between the orbital HOMO and LUMO is favorable [33]. The energy difference between LUMO of benzyl bromide and HOMO of 2*H*-form (ΔE_{gap2} = 5.83 eV) is less than the difference of energy between HOMO of 1*H*-form and LUMO of benzyl bromide (ΔE_{gap1} = 6.03 eV). This confirms that the overall transfer of electron density will shift better from 2*H* form to benzyl bromide (Figure 5).

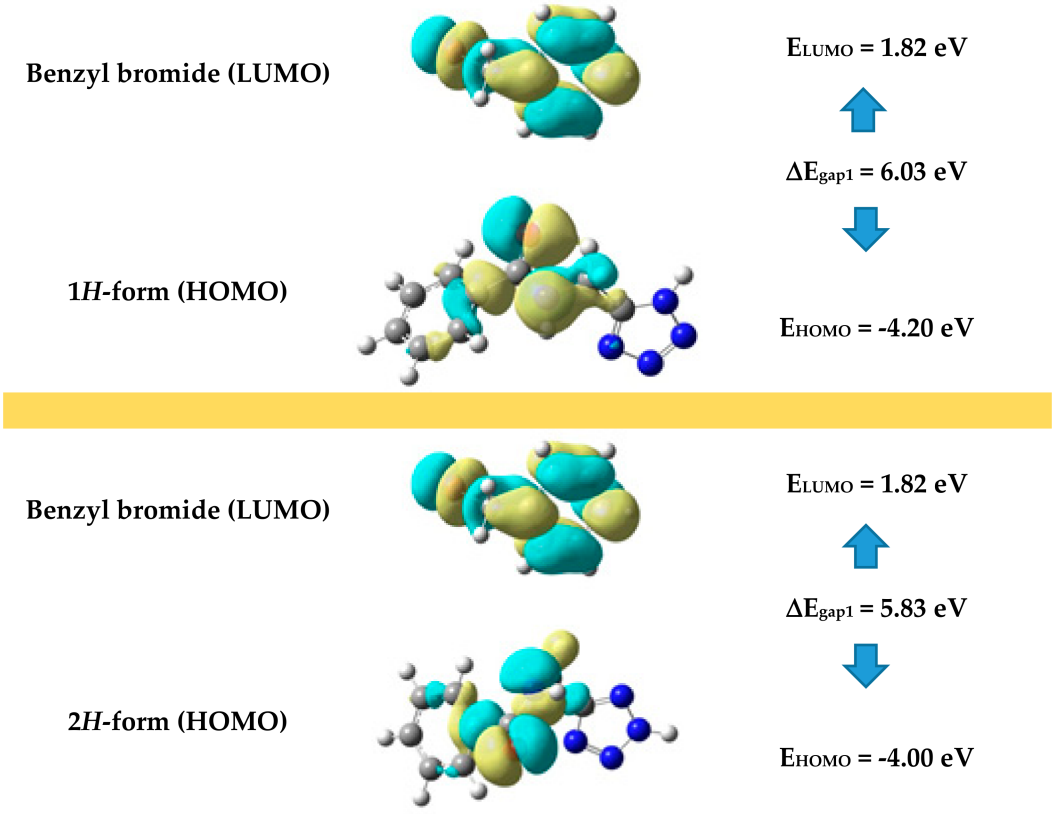

Figure 5. Energy gap between HOMO and LUMO of reagents in path reactions.

The Table 4 shows the HOMO, LUMO and ΔE_{gap} of the two products obtained after the synthesis of 5-AMT. Reading this table shows that the energy gap ($\Delta E = E_{LUMO} - E_{HOMO}$) of the compound 2,5-AMT (ΔE = 0.18 eV) is less than that of 1,5-AMT (ΔE = 0.20 eV). This obviously indicates that the reactivity and stability of compound 2,5-AMT is favorable compared to 1,5-AMT. These results give an argument aspect, reinforcing and explaining the experimental reactions obtained (55% for 2,5-AMT and 45% for 1,5-AMT).

Table 4. Calculated quantum chemical parameters of organic compounds 1,5-AMT and 2,5-AMT using DFT method with 6-31G (d) basis set in aqueous phase.

	ΔH (eV)	E_{LUMO} (eV)	E_{HOMO} (eV)	ΔE (eV)
1,5-AMT	−26,000.25	0.04	−0.15	0.20
2,5-AMT	−26,000.17	0.03	−0.15	0.18

5. Conclusion

In summary, the synthesis of two regioisomers, 1,5- and 2,5-AMTs derivatives was carried out via the *N*-alkylation reaction starting from 5-AMT, which contains a free N-H bond. The purification of these two resulting and the (^{1}H, ^{13}C) NMR study of their spectra allowed us to deduce the tautomeric composition of the starting 5-AMT derivative, and from these NMR spectra studied we deduced 55% for 2,5-AMT alkylation and 45% for 1,5-AMT. DFT calculations also showed that the 2,5-AMT reaction path is more dominant than 1,5-AMT; First, electrostatic potential (ESP) studied showed that the negative regions are delocalized in the nucleophilic sites of the benzyl bromide molecule, while the positive regions are delocalized in the electrophilic zones (blue color) of the two forms of the 5-AMT molecule. Secondly, we have justified that the 2,5-AMT compound is the slightly majority product than the 1,5-AMT product. Finally, the analysis of energy gap ΔE_{gap} showed that the overall transfer of electron density will shift better from 2*H*-form to benzyl bromide. As well as the reactivity and the stability of the compound (2,5-AMT) is favorable compared to (1,5-AMT).

Author Contributions: Conceptualization, Y.A. and A.J.; Methodology, Y.A. and A.J.; Original Draft, Y.A. and A.J.; Writing—Review & Editing, Y.A. and A.J.; Theoretical Calculations, A.J. and A.E.A.; Supervision, A.A. and S.E.I.; visualization, I.B. and A.A.; Validation and formal analysis, Y.A., A.J., A.A., A.E.A., S.E.I. and I.B. All authors have read and agreed to the published version of the manuscript.

Funding: This research received no external funding.

Conflicts of Interest: The authors declare no conflict of interest.

References

1. Gao, F.; Xiao, J.; Huang, G. Current scenario of tetrazole hybrids for antibacterial activity. *Eur. J. Med. Chem.* **2019**, *184*, 111744. [CrossRef]
2. Zhang, J.; Wang, S.; Ba, Y.; Xu, Z. Tetrazole hybrids with potential anticancer activity. *Eur. J. Med. Chem.* **2019**, *178*, 341–351. [CrossRef]
3. Qian, A.; Zheng, Y.; Wang, R.; Wei, J.; Cui, Y.; Cao, X.; Yang, Y. Design, synthesis, and structure-activity relationship studies of novel tetrazole antifungal agents with potent activity, broad antifungal spectrum and high selectivity. *Bioorganic Med. Chem. Lett.* **2018**, *28*, 344–350. [CrossRef]
4. Łukowska-Chojnacka, E.; Kowalkowska, A.; Gizińska, M.; Koronkiewicz, M.; Staniszewska, M. Synthesis of tetrazole derivatives bearing pyrrolidine scaffold and evaluation of their antifungal activity against Candida albicans. *Eur. J. Med. Chem.* **2019**, *164*, 106–120. [CrossRef] [PubMed]
5. Lamie, P.F.; Philoppes, J.N.; Azouz, A.A.; Safwat, N.M. Novel tetrazole and cyanamide derivatives as inhibitors of cyclooxygenase-2 enzyme: Design, synthesis, anti-inflammatory evaluation, ulcerogenic liability and docking study. *J. Enzym. Inhib. Med. Chem.* **2017**, *32*, 805–820. [CrossRef] [PubMed]
6. Tukulula, M.; Sharma, R.-K.; Meurillon, M.; Mahajan, A.; Naran, K.; Warner, D.; Huang, J.; Mekonnen, B.; Chibale, K. Synthesis and Antiplasmodial and Antimycobacterial Evaluation of New Nitroimidazole and Nitroimidazooxazine Derivatives. *ACS Med. Chem. Lett.* **2013**, *4*, 128–131. [CrossRef] [PubMed]
7. Xu, Z.; Gao, C.; Ren, Q.-C.; Song, X.-F.; Feng, L.-S.; Lv, Z.-S. Recent advances of pyrazole-containing derivatives as anti-tubercular agents. *Eur. J. Med. Chem.* **2017**, *139*, 429–440. [CrossRef]
8. Yeung, K.-S.; Qiu, Z.; Yang, Z.; Zadjura, L.; D'Arienzo, C.J.; Browning, M.R.; Hansel, S.; Huang, X.S.; Eggers, B.J.; Riccardi, K.; et al. Inhibitors of HIV-1 attachment Part 9: An assessment of oral prodrug approaches to improve the plasma exposure of a tetrazole-containing derivative. *Bioorg. Med. Chem. Lett.* **2013**, *23*, 209–212. [CrossRef]

9. Dippold, A.A.; Izsák, D.; Klapötke, T.M.; Pflüger, C. Combining the Advantages of Tetrazoles and 1,2,3-Triazoles: 4,5-Bis(tetrazol-5-yl)-1,2,3-triazole, 4,5-Bis(1-hydroxytetrazol-5-yl)-1,2,3-triazole, and their Energetic Derivatives. *Chem. A Eur. J.* **2016**, *22*, 1768–1778. [CrossRef]
10. Fischer, D.; Klapötke, T.M.; Stierstorfer, J. 1,5-Di (nitramino) tetrazole: High Sensitivity and Superior Explosive Performance. *Angew. Chem. Int. Ed.* **2015**, *54*, 10299–10302. [CrossRef]
11. Fischer, N.; Karaghiosoff, K.; Klapötke, T.M.; Stierstorfer, J. Stierstorfer, J. New Energetic Materials featuring Tetrazoles and Nitramines—Synthesis, Characterization and Properties. *Z. Anorg. Allg. Chem.* **2010**, *636*, 735–749. [CrossRef]
12. Matta, C.F.; Arabi, A.A.; Weaver, D.F. The bioisosteric similarity of the tetrazole and carboxylate anions: Clues from the topologies of the electrostatic potential and of the electron density. *Eur. J. Med. Chem.* **2010**, *45*, 1868–1872. [CrossRef] [PubMed]
13. Malik, M.A.; Wani, M.Y.; Al-Thabaiti, S.A.; Shiekh, R.A. Tetrazoles as carboxylic acid isosteres: Chemistry and biology. *J. Incl. Phenom. Macrocycl. Chem.* **2014**, *78*, 15–37. [CrossRef]
14. Araujo-Andrade, C.; Reva, I.; Fausto, R. Tetrazole acetic acid: Tautomers, conformers, and isomerization. *J. Chem. Phys.* **2014**, *140*, 064306. [CrossRef]
15. Yuan, H.; Silverman, R.B. New substrates and inhibitors of γ-aminobutyric acid aminotransferase containing bioisosteres of the carboxylic acid group: Design, synthesis, and biological activity. *Bioorganic Med. Chem.* **2006**, *14*, 1331–1338. [CrossRef]
16. Schwarz, J.B.; Colbry, N.L.; Zhu, Z.; Nichelson, B.; Barta, N.S.; Lin, K.; Hudack, R.A.; Gibbons, S.E.; Galatsis, P.; DeOrazio, R.J.; et al. Carboxylate bioisosteres of pregabalin. *Bioorganic Med. Chem. Lett.* **2006**, *16*, 3559–3563. [CrossRef]
17. Kiselev, V.G.; Cheblakov, P.B.; Gritsan, N.P. Tautomerism and Thermal Decomposition of Tetrazole: High-Level ab Initio Study. *J. Phys. Chem. A* **2011**, *115*, 1743–1753. [CrossRef]
18. Wong, M.W.; Leung-Toung, R.; Wentrup, C. Tautomeric equilibrium and hydrogen shifts of tetrazole in the gas phase and in solution. *J. Am. Chem. Soc.* **1993**, *115*, 2465–2472. [CrossRef]
19. Elkin, M.; Newhouse, T.R. Computational chemistry strategies in natural product synthesis. *Chem. Soc. Rev.* **2018**, *47*, 7830–7844. [CrossRef]
20. Pérez, P.; Domingo, L.R.; Duque-Noreña, M.; Chamorro, E. A condensed-to-atom nucleophilicity index. An application to the director effects on the electrophilic aromatic substitutions. *J. Mol. Struct. THEOCHEM* **2009**, *895*, 86–91. [CrossRef]
21. Berionni, G.; Pégot, B.; Goumont, R. Theoretical and experimental 1H, 13C and 15N NMR studies of N-alkylation of substituted tetrazolo [1,5-a] pyridines. *Magn. Reson. Chem.* **2010**, *48*, 101–110. [CrossRef]
22. Kroon, E.; Schulze, J.O.; Süß, E.; Camacho, C.J.; Biondi, R.M.; Dömling, A. Discovery of a potent allosteric kinase modulator by combining computational and synthetic methods. *Angew. Chem.* **2015**, *127*, 14139–14142. [CrossRef]
23. Parr, R.G.; Pearson, R.G. Absolute hardness: Companion parameter to absolute electronegativity. *J. Am. Chem. Soc.* **1983**, *105*, 7512–7516. [CrossRef]
24. Parr, R.G.; Szentpály, L.v.; Liu, S. Electrophilicity Index. *J. Am. Chem. Soc.* **1999**, *121*, 1922–1924. [CrossRef]
25. Domingo, L.R.; Chamorro, E.; Pérez, P. Understanding the Reactivity of Captodative Ethylenes in Polar Cycloaddition Reactions A Theoretical Study. *J. Org. Chem.* **2008**, *73*, 4615–4624. [CrossRef]
26. Frisch, A.M.J.; Trucks, G.W.; Schlegel, H.B.; Scuseria, G.E.; Robb, M.A.; Cheeseman, J.R.; Scalmani, G.; Barone, V.; Mennucci, B.; Petersson, A.G.; et al. *Fox*; Gaussian, Inc.: Wallingford, CT, USA, 2009.
27. Schüürmann, G.; Cossi, M.; Barone, V.; Tomasi, J. Prediction of the p K a of carboxylic acids using the ab initio continuum-solvation model PCM-UAHF. *J. Phys. Chem. A* **1998**, *102*, 6706–6712. [CrossRef]
28. Parr, R.; Yang, W. *Density Functional Theory of Atoms and Molecules*; Oxford University Press: New York, NY, USA, 1989.
29. Domingo, L.R.; Ríos-Gutiérrez, M.; Pérez, P. Applications of the Conceptual Density Functional Theory Indices to Organic Chemistry Reactivity. *Molecules* **2016**, *21*, 748. [CrossRef] [PubMed]
30. Aouine, Y.; Aarab, N.; Alami, A.; El Hallaoui, A.; Ebn Touhami, M.; Elachqar, A.; Sfaira, M.; Faraj, H. Synthesis and characterization of novel 5-substituted tetrazoles having an inhibiting activity of corrosion for mild steel in the acidic media. *Moroc. J. Heterocycl. Chem.* **2015**, *10*. [CrossRef]
31. Elguero, J.; Marzin, C.; Roberts, J.D. Carbon-13 magnetic resonance studies of azoles. Tautomerism, shift reagent effects, and solvent effects. *J. Org. Chem.* **1974**, *39*, 357–363. [CrossRef]
32. Sveshnikov, N.N.; Nelson, J.H. Discrimination of Structural Isomers of N-Methylated and N-tert-Butylated Tetrazoles by 13C and 15N NMR. Long-Range 15N,1H Coupling Constants. *Magn. Reson. Chem.* **1997**, *35*, 209–212. [CrossRef]
33. Jmiai, A.; El Ibrahimi, B.; Tara, A.; Oukhrib, R.; El Issami, S.; Jbara, O.; Bazzi, L.; Hilali, M. Chitosan as an eco-friendly inhibitor for copper corrosion in acidic medium: Protocol and characterization. *Cellulose* **2017**, *24*, 3843–3867. [CrossRef]